ADVANCED ENGINEERING MATERIALS
www.aem-journal.com

Exploiting Functionally Graded Elastomeric Materials to Program Collapse and Mechanical Properties

*Charles El-Helou and Ryan L. Harne**

The development of materials with periodic microstructures provides the means to tune mechanical properties via prescribed collapse mechanisms. As investigations give attention to tunable unit cell designs, questions arise regarding strategic ways to exploit built-up materials to empower large, programmable control over properties and material functionality. The potential to rationally design functionally graded elastomeric materials to yield prescribed mechanical properties is demonstrated herein. Following computational and experimental studies of simplified unit cells and layers, the results inspire ways to exploit linear elastic network analogies to design built-up and functionally graded materials. This approach exemplifies a streamlined means to create pre-programmed properties on the basis of simple calculations related to measurements from fundamental material constituents. The results build a foundation for innovative approaches to newly leverage elastomeric materials with programmable collapse for myriad engineering applications.

Emerging interest to broaden the toolset of design for advanced materials has led to numerous material concepts for packaging, structural damping, vibration attenuation, and so on. For such practices, the mechanical properties of the materials ideally exhibit low dynamic stiffness.[1–3] To achieve this target, lightweight elastomer-based materials with cellular, mesoscale void patterns are recently exploited.[4–7] Through the collapse and deformation of the network of beams realized in the void patterns, researchers are uncovering innovative ways to shape and manipulate the mechanical properties of such elastomeric materials.[8–12] When subjected to dynamic loads, reversible elastic buckling and low dynamic stiffness effected in the microscale beam networks lead to controlled elastic energy absorption and wave propagation.[13–17] In addition, by scrutinizing the interplay between viscosity and elasticity, cellular elastomeric materials composed from viscoelastic polymers may be tailored to mitigate high-rate shock and vibration by reducing dynamic stiffness and increasing macroscopic damping.[18–22] All together, the discoveries underscore the fact that the mechanical properties of engineered materials may be far more versatile than those of the underlying bulk material.

C. El-Helou, Prof. R. L. Harne
Department of Mechanical and Aerospace Engineering
The Ohio State University
Columbus, OH 43210, USA
E-mail: harne.3@osu.edu

The ORCID identification number(s) for the author(s) of this article can be found under https://doi.org/10.1002/adem.201900807.

DOI: 10.1002/adem.201900807

Yet, recent attention is turned to devise techniques for passive adaptation of such non-natural material behavior to enhance the multifunctionality and versatility. In particular, multistability and layering are shown to adapt mechanical properties through the ordered triggering of collapse events within the material void patterns.[13,23–25] The ways by which such design factors enable control of properties are unique for each mesoscale void pattern considered in the engineered material. This research sees potential in the "X"-shaped beam network studied by Bunyan and Tawfick.[26] The antagonistic crossing of beam elements in this particular void pattern, **Figure 1**a, enables collapse by rotation of the patterned unit cell in a layer, Figure 1d. Yet despite emerging knowledge on such unit cell behavior, it is well known that periodic materials with finite extents exhibit mechanical and dynamic properties essentially governed by the boundary conditions.[27] Consequently, there remain needs to articulate techniques to formulate and characterize built-up, graded, and adaptive variants of this material platform. While researchers have begun shedding light on the parametric design of additively manufactured materials that exhibit multiple states of collapse,[28,29] the soft matter realization of the functionally graded material examined here represents a far different local deformation field characterized by continuous conformations and total self-contact, not represented in the 3D-printed realizations. As a result, a modeling framework is required to understand the parameters and designs that govern collapse in functionally graded soft material systems.

Motivated by this knowledge gap, in this report, we investigate mechanisms that give rise to programmable control of mechanical properties in functionally graded elastomeric materials having layered, crossed beam networks realized by mesoscale voids, Figure 1. Here, we specifically exploit functional gradients by stacking layers of unit cells, Figure 1b. For instance, by tailoring the beam thicknesses from 0.80 to 1.00 mm and then to 1.20 mm for layers of unit cells, Figure 1b, the mechanical properties in Figure 1c and photographs in Figure 1e reveal a sequential collapse behavior that is qualitatively and quantitatively not manifest in the material having the single layer of periodic unit cells with beam thicknesses of 1 mm, Figure 1c,d. Essentially nonlinear stiffness is realized in these collapse events,[26] such as in Figure 1c where the slope of the curves is nearly zero. Through leveraging such functional gradients in layers of unit cells having crossed beam networks, we find that substantial control over the material behavior is empowered. On the other hand, we also find that the

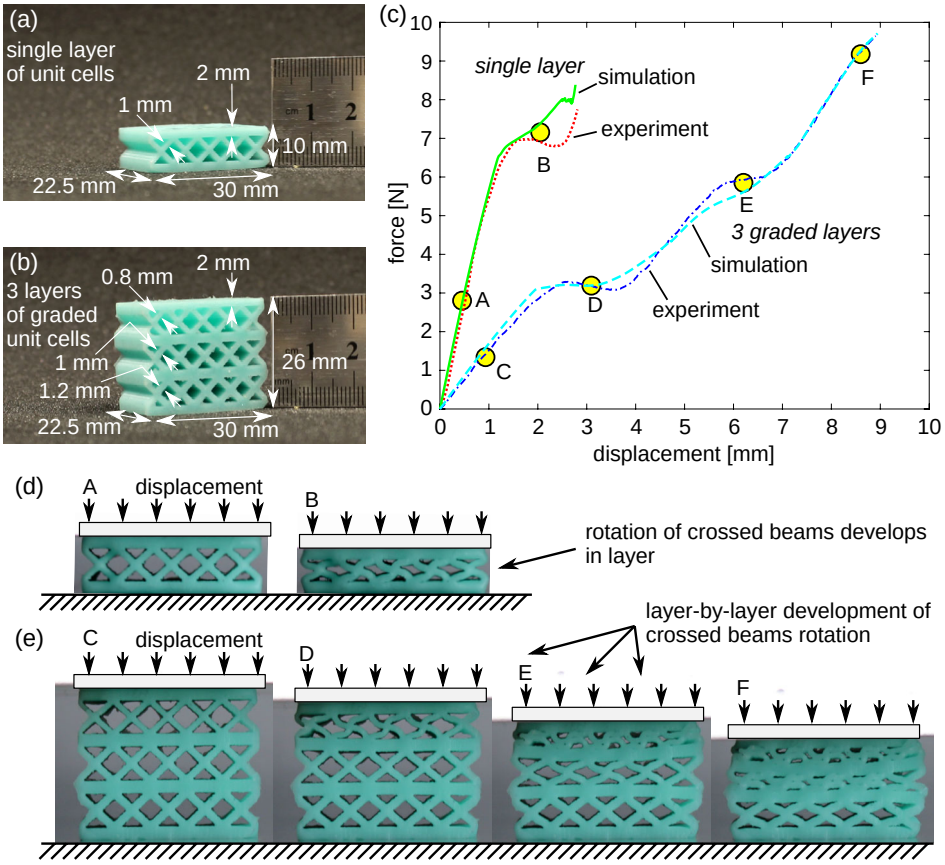

Figure 1. Functional gradients broaden the range of mechanical properties adaptation. Geometry of elastomeric materials with a) a single layer of unit cells and b) three layers of functionally graded unit cells. c) Mechanical properties of the materials as determined by experiments and simulation. Photographs of deformation for the d) single-layer material and e) functionally graded layer material. Labels in (d,e) correspond to points in mechanical properties in (c).

sequence of collapse is not determined by a linear superposition of collapsing layers because the critical displacement and force of the single-layer collapse event are not critical points in the mechanical properties of the graded material. In the initial uniaxial compression regime shown in Figure 1c, it is apparent that individual layers in the functionally graded multilayer geometry do not behave independently. As such, a need exists to illuminate the origins of such nonaffine behavior and to understand techniques to capitalize on the unique material system characteristics. In this report, we utilize integrated computational and experimental investigations to shed light on the intriguing mechanisms of collapse and programmable mechanical properties in this new class of functionally graded elastomeric material.

The material samples studied in this report are fabricated by casting a platinum cure silicone rubber (Smooth-On Mold Star 15S) in 3D-printed acrylonitrile butadiene styrene (ABS) molds (FlashForge Creator Pro) bearing the negative of the sample shape to be tested. The materials are cured at room temperature and room pressure. Samples are demolded and then aerated for 24 h prior to experimental study. The mechanical properties are examined in a load frame (ADMET eXpert 5600) where the actuator uniaxially guides a rigid platen attached to a load cell (PCB 110205A) while displacing at a rate of 0.5 mm min^{-1}. A laser displacement sensor (Micro-Epsilon optoNCDT ILD1700-200) provides readout of the load cell position as the rigid platen compresses the samples quasi-statically.

To look deeper into the mechanics of the layered elastomeric materials, we generate finite-element (FE) models that emulate the experimental protocol. ABAQUS Dynamic-Implicit simulations are conducted with 2D plane strain models, warranted on the basis of the deep and constant material cross section. We use a hyperelastic Neo–Hookean material model with empirically determined Young's modulus of 476 kPa and Poisson's ratio of 0.499 for the samples considered here. The model boundary conditions are similar to the boundaries of the material cross section in experiment. The bottom surface in the model is fixed, whereas the top surface displaces only in the vertical direction. As evidenced in the simulation results of mechanical properties, Figure 1c, the simulations qualitatively reproduce the stiffness plateau regions observed in the experimental results. The agreement is particularly seen in terms of the critical displacements and critical forces at which the bifurcations occur in the mechanical properties. Discrepancies between the measurements and predictions may be associated with the presence of minor defects through the fabricated cross section, which do not, otherwise, detract from the overall agreement among the salient trends in the data.

To begin a detailed investigation of material behavior evident from layers of unit cells, the contrasts among mechanical properties of unit cells and layer assemblies are studied. The specific crossed beam unit cell geometry studied here has considerably shorter height than unit cells studied in the previous study.[26] In addition, the previous study[26] did not investigate assemblies of the unit cells, instead giving attention to the unit cell in isolation. Here, we scrutinize the ramifications of unit cell assembly, especially boundary influences. **Figure 2**a shows the unit cell geometry considered in this report and illustrates how the geometry relates to a layer assembly. The unit cell has 1.00 mm thick beams crossed over a 6 mm lateral extent and is bounded on top and bottom by 1 mm thick beams to make a unit cell of 8 mm total height and 6 mm total width, Figure 1a. FE simulations of uniaxial compression are undertaken, and the resulting mechanical properties are shown in Figure 2b. For the unit cell results, periodic boundary conditions are imposed on all leftmost and rightmost boundaries, whereas free boundaries at these same locations are used for simulations of layer material assemblies. Figure 2b shows that the periodic unit cell exhibits a well-defined collapse and plateau in the mechanical properties. This behavior is associated with the rotation of the crossed beams in each unit cell composing the deformed layer, evident by comparing labels A and B in Figure 2c corresponding to pre- and post-collapse in Figure 2b.

To explore the effects of periodic assembly of the unit cell, we design single-layer materials having 3, 5, 8, or 20 unit cells. Here, to uncover factors that influence the layer assemblies, we consider each unit cell to be an analogous elastic network of linear springs k_h and k_x in series, Figure 2c. The elastic spring k_h is the uniaxial spring stiffness of the top or bottom horizon elastomer segments of the unit cell, whereas k_x is the uniaxial spring stiffness of the crossed beam component. As a result, the layers are considered to be parallel assemblies of such linear elastic units, Figure 2d. This assumption is supported on the basis of the FE simulations in Figure 2b that exemplify nearly linear behavior prior to collapse for the assemblies of unit cells. For the ideal elastic network, Hooke's Law suggests that the force per unit cell does not change with the change in the number of unit cells assembled in the layer. Yet, as shown in Figure 2b, the number of unit cells in the layer influences the force experienced per unit cell in the material. In particular, with the increase in the number of unit cells from 3 to 5 to 8 and then to 20, the mechanical properties progressively converge to those of the unit cell modeled with periodic boundary conditions.

The deviation of this trend with respect to Hooke's Law is due to boundary influences that more strongly affect material layers having smaller numbers of assembled unit cells. For instance, Figure 2d shows that the layer having five unit cells reveals consistent collapse behavior for the innermost three unit cells,

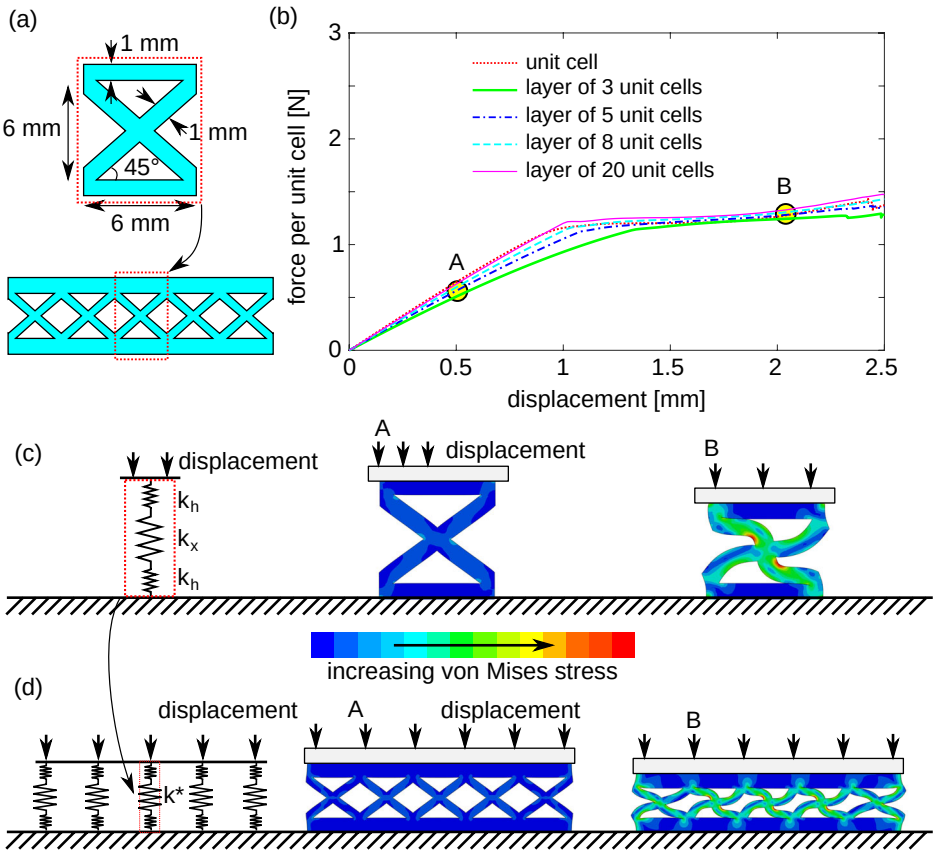

Figure 2. Relation of layered assembly and periodic unit cell behaviors. a) Schematic of unit cell geometry and assembly technique for a layer. b) Mechanical properties per unit cell determined by the FE model. Schematic of the analogous elastic network and the associated deformation before and after collapse for c) the unit cell and d) an assembly of five unit cells in a layer. In (c,d), the color shading of simulation results is the von Mises stress.

whereas the outermost two unit cells do not rotate in a way consistent with the innermost response. Consequently, the boundaries inherent in finite assemblies of the crossed beam type unit cells strongly influence the material behavior and mechanical properties.

When assembled by stacking identical layers, the elastomeric material exhibits multiple collapse behaviors originally evidenced in Figure 1e. As shown in **Figure 3**a, the effects of periodic assembly of layers are explored by comparing FE simulations where layers of five identical unit cells are assembled with varied number of stacked layers. A 2 mm thick horizontal elastomer segment separates each layer. The simulation results in Figure 3b illustrate a progressive collapse of the layers occurring near the same force in all the materials. For materials assembled from three, five, or seven layers, the critical displacements and forces are similar when contrasted to the differing critical displacement for the single layer of unit cells. As shown in Figure 3c, such trend is associated with the lack of interlayer deformation field in the single layer that is observed by bending of the horizontal elastomer segments in the multilayer materials. These results suggest that the multilayer materials pose distinct opportunity to tailor mechanical properties. To capitalize on this opportunity, a predictive tool is necessary to accelerate an informed design process.

Again using the elastic network analogy, we expand the concept to predict the mechanical properties of multilayer materials. Here, we exemplify the elastic network predictive tool for the three-layer material shown in **Figure 4**a where all unit cells are identical. A formal modeling approach is described in the Supporting Information that establishes the relationships among the unit cell constituents, layer assembly, and material gradients with the corresponding approximated mechanical properties. The model requires simplified unit cell FE simulation results specifically for the linear uniaxial stiffness prior to collapse, and the critical displacement and critical force at collapse, and the uniaxial stiffness after collapse. To leverage the predictive capability for the material in Figure 4a, the unit cell uniaxial stiffness k^* is found to be 1.28 kN m^{-1}, and the critical force f_c is found to be 1.14 N. The uniaxial stiffnesses for the three layers of the material in Figure 4b are nominally the same, so that $k_1^* = k_2^* = k_3^* = 1.28\,\text{kN m}^{-1}$.

As the simulation results (red dashed) of the mechanical properties in Figure 4a agree well with experimental measurements (green solid), the calculated results are compared with the simulations. The uniaxial stiffness determined using the spring analogy for the three-layer material in Figure 4c is approximated to be 2.13 kN m^{-1}, whereas the stiffness determined from FE simulation is 1.51 kN m^{-1}. Furthermore, the critical displacement determined using the elastic network approximation is also 2.68 mm, whereas the simulated critical displacement is 3.62 mm. Such discrepancy is due to nonuniform unit cell collapse in the multicellular geometry. The origins of such discrepancies are evident in the deformed material states shown in Figure 4c,d. In particular,

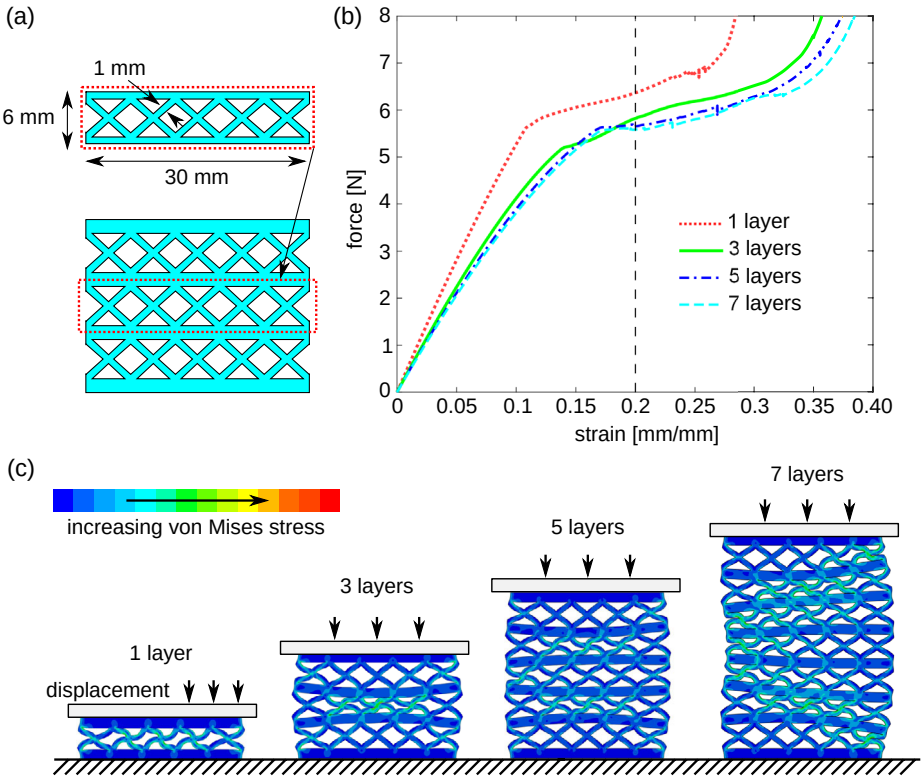

Figure 3. Relation of vertical periodic layers quantity on collapse behavior. a) Schematic of five unit cell layer and assembly technique for a multilayer material. b) Mechanical properties determined by the FE model. c) Simulation results illustrating a von Mises stress at 0.2 mm mm^{-1} strain for the one, three, five, and seven layer materials.

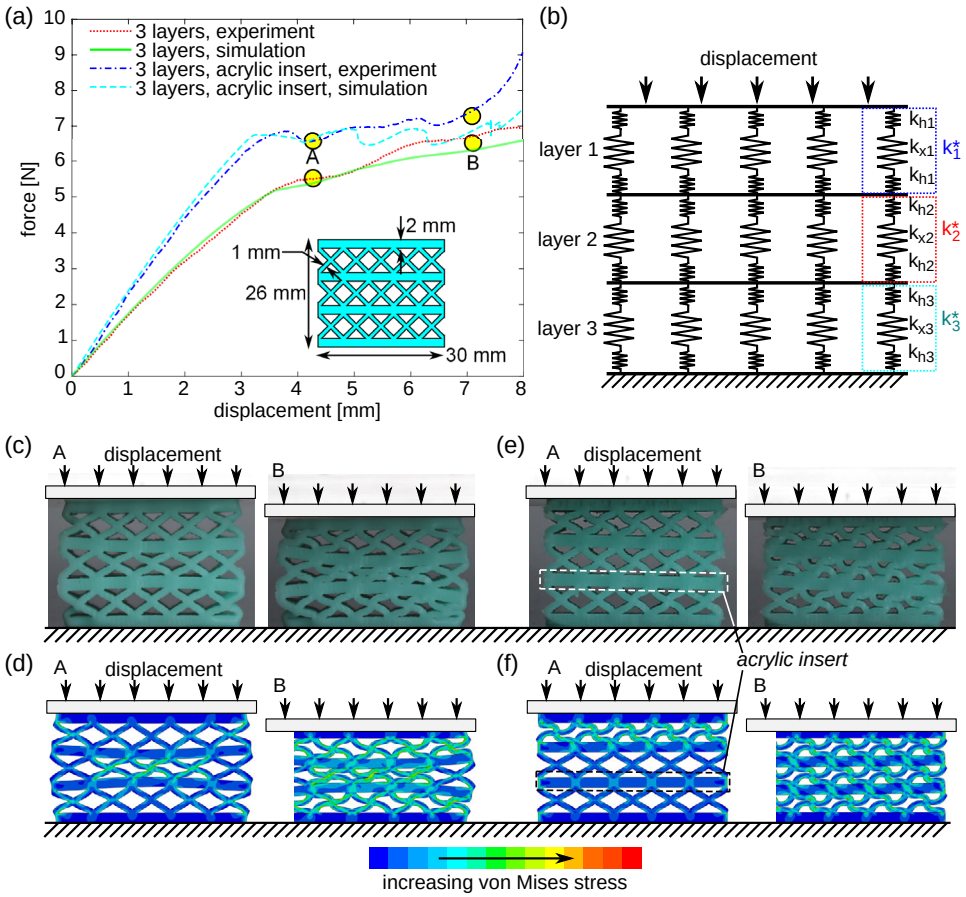

Figure 4. Programming uniaxial stiffness by layer interfaces. a) Mechanical properties of three-layer materials determined by the FE model and experiments. Three-layer material geometry shown in the inset as well as b) a schematic of its analogous elastic network. Photographs of deformation of the three-layer materials having c) elastomer horizontal segments and e) elastomer-covered acrylic horizontal segments. Corresponding FE simulation results with von Mises stress contour overlays for three-layer materials having d) elastomer horizontal segments and f) elastomer-covered acrylic horizontal segments. Labels (c,d,e,f) correspond to labels in (a).

the horizontal elastomer segments exhibit excessive bending that inhibits the unit cell-like rotation after collapse of all of the unit cells in a layer, Figure 2b,c.

To confirm that deviation in the predicted uniaxial stiffness and critical collapse characteristics result from the deformation of the horizontal elastomer segments, we fabricate multilayer materials having nearly rigid horizontal members. In particular, we overmold laser-perforated acrylic with elastomer during the curing process of the whole material. The resulting materials have acrylic inserts in each horizontal segment, thus drastically diminishing the deformation of the horizontal segments. To incorporate the perforated acrylic layers in the FE model, we assign the linear elastic horizontal segment material to have Young's modulus of 2.8 MPa and Poisson's ratio of 0.37. Young's modulus value is less than bulk acrylic due to the elastomer filled holes fabricated in the acrylic that are found to substantially reduce Young's modulus from bulk values. Figure 4a compares the simulation and experimental results for the three-layer material having the acrylic inserts. While the simulations accurately predict the linear elastic stiffness, more notable dynamic stiffness changes follow each collapse event compared with the measurements. In addition, the overall critical force level and critical displacement range are in good agreement and shift considerably compared with the multilayer material without the nearly rigid acrylic inserts. Qualitatively, the deformation characteristics of the three-layer material with acrylic inserts agree well comparing FE simulations and measurements, Figure 4e,f.

Furthermore, the linear elastic network approximation of uniaxial stiffness and critical collapse characteristics is greatly improved with the introduction of the acrylic inserts. To compute the linear elastic uniaxial stiffness of the multilayer material with acrylic inserts, the unit cell stiffness k^* is found from unit cell FE simulations lacking the top and bottom horizontal beam segments, leading to $k^* = 1.55\,\mathrm{kN\,m^{-1}}$. In addition, the horizontal elastomer segments are modeled as rigid layers in the elastic network model. Using these results, the calculated prediction of the uniaxial stiffness of the multilayer material with acrylic inserts is $2.38\,\mathrm{kN\,m^{-1}}$ compared with the simulation result of $2.62\,\mathrm{kN\,m^{-1}}$, resulting in a 9.3% deviation and a 31.7% improvement in prediction when compared with the nonacrylic material. Similarly, the approximated critical displacement is computed to be 2.94 mm, whereas the simulated critical displacement is 3.20 mm. These

findings help to uncover the relations among unit cell characteristics that result in critical collapse events and assembly details that culminate in multilayer elastomeric materials with distinctive collapse behaviors for tuning mechanical properties.

Having gained understanding on factors that give rise to assembled multilayer material properties, we explore functional gradients of the patterned unit cell geometry as an approach to test the extensibility of the linear elastic network design methodology. In fact, functional gradients may be realized by any form of local property variation and not only by the geometric changes studied here in the layer stacking sequence of unit cells. Intuitively, unit cells having different crossed beam thicknesses lead to different critical collapse characteristics;[26] thus, functional gradients may exemplify straightforward ways to cultivate broad control over mechanical properties. Here, we change the crossed beam thicknesses in layers that include five unit cells each. The material is then an assembly of three layers. The inset of **Figure 5**a shows the material geometry considered here. The crossed beam thickness changes from 0.8 mm in the topmost layer to 1 mm in the middle layer and then to 1.2 mm in the bottommost layer. Materials are likewise fabricated and simulated with and without acrylic inserts in the horizontal segments.

For the materials in Figure 5, three pronounced collapse events transpire sequentially at distinct critical displacements and forces. Furthermore, each collapse and layerwise rotation introduces a finite loading range where low dynamic stiffness is achieved. For the material with acrylic inserts, the collapse events are well defined and may result in negative dynamic stiffness, Figure 5a, e.g., label A. Dynamic cycling around these collapse events may yield hysteresis desirable for energy dissipation,[30] although parametric designs that maximize this functionality are a subject for continuing research. Comparing the functionally graded materials with and without the acrylic inserts in Figure 5a, the introduction of the stiffer horizontal segments by the embedded acrylic globally stiffens the material, so that the collapse events uniformly occur at higher critical forces and less critical displacement than without the nearly rigid interfacing segments. Notably, the horizontal segments remain mostly horizontal during and after each collapse event, Figure 5b,c, justifying the assumptions made in the modeling and elastic network analogy.

The linear elastic network approximation is likewise used to predict the resulting mechanical properties and critical collapse characteristics of the functionally graded materials. Full modeling details are provided in the Supporting Information, and in this case, the model is more effectively described as piecewise linear due to the resulting formulation of the predicted mechanical properties, Figure S2, Supporting Information. Here, the layerwise uniaxial stiffnesses are different, so that $k_1^* \neq k_2^* \neq k_3^*$. The linear elastic uniaxial stiffnesses of the unit cells are 1.16, 1.55, and 2.03 kN m^{-1} for the functionally graded material with acrylic inserts. Furthermore, following the collapse of each layer, the stiffness of the compacted unit cells is determined from the unit cell FE results in Figure 2b to likewise calculate the second and third critical points. These linear elastic uniaxial stiffnesses are 4.95 and 5.15 kN m^{-1} for the 0.8 and 1.0 mm unit cell beam thicknesses, respectively. Using the network analogy, we estimate the first, second, and third critical force to be 3.84, 7.58, and 14.80 N, respectively, compared with the simulated critical forces of 3.55, 6.69, and 11.51 N. Thus, the absolute errors in critical forces are 7.5%, 11.7%, and 22.2%. In addition, the first, second, and third estimated critical displacements are 1.53, 5.74, and 9.43 mm compared with the simulated critical displacement of 1.60, 5.52, and 7.88 mm, respectively. In this case, absolute errors for critical displacement predictions are 4.5%, 3.8%, and 16.4%. It is evident from the results that the 1D linear elastic network model predicts the first critical conditions with relatively high accuracy, whereas the error generally increases with increasing the number of stacked layers. Such insights give designers a broad freedom to develop functionally graded elastomeric materials with programmable mechanical properties and collapse characteristics on the basis of fundamental information for the material constituents.

In summary, we demonstrate the potential to rationally design functionally graded elastomeric materials to yield prescribed mechanical properties, including low dynamic stiffness. We find analogies between the basic unit cell composition and linear elastic components, inspiring a representation of the whole, layered,

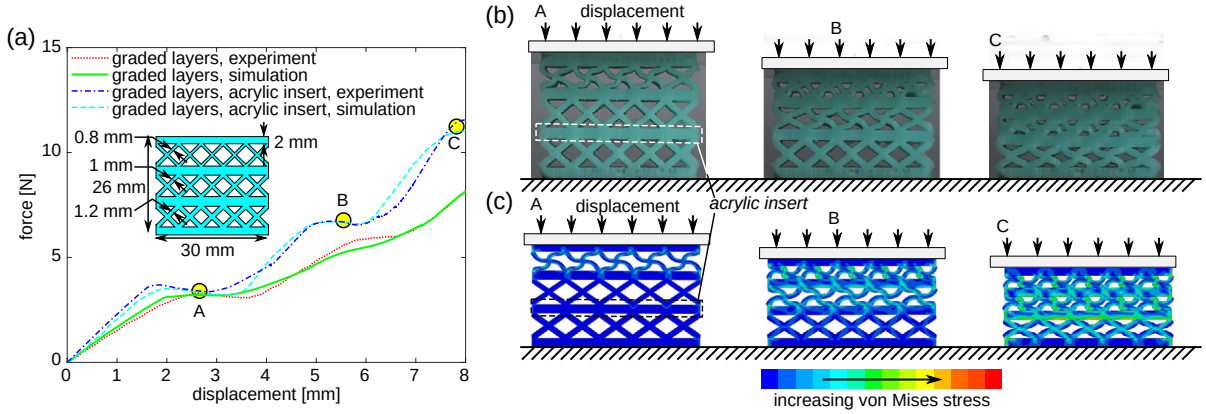

Figure 5. Functionally graded materials with programmable collapse. a) Mechanical properties of functionally graded three-layer materials determined by the FE model and experiments. Layer material geometry shown in inset. b) Photographs of deformation of the functionally graded three-layer materials having elastomer-covered acrylic horizontal segments. c) Corresponding FE simulation results with von Mises stress contour overlays. Labels (b,c) correspond to labels in (a).

and finite material as an assembled elastic network. With such insight, the mechanical properties and points of criticality are relatively straightforward to approximate with sufficient degree of fidelity to be compared with experimental data. These results empower the design of intricate and built-up material systems with pre-programmed properties on the basis of simple calculations related to measurements from fundamental material constituents. Based on the low dynamic stiffness achieved, these materials may advance future applications requiring broadband vibration isolation and controlled wave propagation.[13,15,16]

Supporting Information

Supporting Information is available from the Wiley Online Library or from the author.

Acknowledgements

This research is supported in part by the member organizations of the NSF I/UCRC Smart Vehicle Concepts Center, a National Science Foundation Industry/University Cooperative Research Center created under grant NSF IIP-1238286.

Conflict of Interest

The authors declare no conflict of interest.

Keywords

elastomeric materials, functionally graded materials, programmable mechanical properties

Received: July 4, 2019
Revised: August 26, 2019
Published online: October 14, 2019

[1] I. A. Karnovsky, E. Lebed, in *Theory of Vibration Protection*, Springer, Berlin **2016**, pp. 653–657.
[2] M. Aykan, M. Çelik, *Mech. Syst. Signal Process.* **2009**, *23*, 897.
[3] S. Otari, S. Odof, J. B. Nolot, P. Vasseur, J. Pellot, N. Krajka, D. Erre, *Packag. Technol. Sci.* **2011**, *24*, 177.
[4] K. Bertoldi, M. C. Boyce, S. Deschanel, S. M. Prange, T. Mullin, *J. Mech. Phys. Solids* **2008**, *56*, 2642.
[5] B. G. Compton, J. A. Lewis, *Adv. Mater.* **2014**, *26*, 5930.
[6] T. A. Schaedler, W. B. Carter, *Annu. Rev. Mater. Res.* **2016**, *46*, 187.
[7] S. C. Han, J. W. Lee, K. Kang, *Adv. Mater.* **2015**, *27*, 5506.
[8] J. T. B. Overvelde, K. Bertoldi, *J. Mech. Phys. Solids* **2014**, *64*, 351.
[9] K. Bertoldi, *Annu. Rev. Mater. Res.* **2017**, *47*, 51.
[10] S. Babaee, J. Shim, J. C. Weaver, E. R. Chen, N. Patel, K. Bertoldi, *Adv. Mater.* **2013**, *25*, 5044.
[11] E. B. Duoss, T. H. Weisgraber, K. Hearon, C. Zhu, W. Small, T. R. Metz, J. J. Vericella, H. D. Barth, J. D. Kuntz, R. S. Maxwell, C. M. Spadaccini, T. S. Wilson, *Adv. Funct. Mater.* **2014**, *24*, 4905.
[12] J. T. B. Overvelde, S. Shan, K. Bertoldi, *Adv. Mater.* **2012**, *24*, 2337.
[13] S. Shan, S. H. Kang, J. R. Raney, P. Wang, L. Fang, F. Candido, J. A. Lewis, K. Bertoldi, *Adv. Mater.* **2015**, *27*, 4296.
[14] S. Rudykh, M. C. Boyce, *Phys. Rev. Lett.* **2014**, *112*, 034301.
[15] R. L. Harne, Z. Wu, K. W. Wang, *J. Mech. Des.* **2016**, *138*, 021402.
[16] S. Shan, S. H. Kang, P. Wang, C. Qu, S. Shian, E. R. Chen, K. Bertoldi, *Adv. Funct. Mater.* **2014**, *24*, 4935.
[17] K. Bertoldi, M. C. Boyce, *Phys. Rev. B* **2008**, *77*, 052105.
[18] S. Cui, R. L. Harne, *Int. J. Solids Struct.* **2018**, *135*, 197.
[19] P. Vuyk, S. Cui, R. L. Harne, *Adv. Eng. Mater.* **2018**, *20*, 1700828.
[20] T. Frenzel, C. Findeisen, M. Kadic, P. Gumbsch, M. Wegener, *Adv. Mater.* **2016**, *28*, 5865.
[21] J. Bishop, Q. Dai, Y. Song, R. L. Harne, *Adv. Eng. Mater.* **2016**, *18*, 1871.
[22] N. Hu, R. Burgueño, *Smart Mater. Struct.* **2015**, *24*, 063001.
[23] J. Meaud, K. Che, *Int. J. Solids Struct.* **2017**, *122–123*, 69.
[24] D. Restrepo, N. D. Mankame, P. D. Zavattieri, *Extreme Mech. Lett.* **2015**, *4*, 52.
[25] I. Maskery, A. Hussey, A. Panesar, A. Aremu, C. Tuck, I. Ashcroft, R. Hague, *J. Cell. Plast.* **2017**, *53*, 151.
[26] J. Bunyan, S. Tawfick, *Adv. Eng. Mater.* **2019**, *21*, 1800791.
[27] E. A. Matsumoto, R. D. Kamien, *Phys. Rev. E* **2009**, *80*, 021604.
[28] H. Yang, L. Ma, *J. Mater. Sci.* **2019**, *54*, 3509.
[29] K. Che, C. Yuan, J. Wu, J. Qi, J. Meaud, *J. Appl. Mech.* **2017**, *84*, 011004.
[30] N. Kidambi, R. L. Harne, K. W. Wang, *J. Vib. Acoust.* **2016**, *138*, 011001.

Supporting Information

Exploiting functionally graded elastomeric materials to program collapse and mechanical properties

*Charles El-Helou and Ryan L. Harne**

Department of Mechanical and Aerospace Engineering, The Ohio State University, Columbus, OH 43210
E-mail: harne.3@osu.edu

1 Elastic Network Model

1.1 Periodic Multilayer Material

Using a one-dimensional elastic network analogy derived from Hooke's law, a model is first employed to predict the linear uniaxial stiffness, critical displacements, and critical forces of the materials. For sake of example, a material is investigated possessing 3 identically designed layers, and thus perfectly periodic, with 5 unit cells per layer, as seen in Figure 4 of the main text. The linear elastic uniaxial stiffness of the i^{th} unit cell k_i^* is approximated by Equation (1), where k_h is the uniaxial stiffness of the horizontal elastomer segment and k_x is the uniaxial stiffness of the crossed beam component.

$$k_i^* = \left[\frac{1}{k_h} + \frac{1}{k_x} + \frac{1}{k_h} \right]^{-1} \tag{1}$$

In this investigation, we extract k_i^* from the slope of the linear uniaxial regime of the unit cell FE simulation, i.e. from Figure 2(b) in the main text. The uniaxial stiffnesses for all units cells in this 3 layer material example are nominally the same. To determine the critical displacement at which a collapse event occurs for the multilayer material, the nodal displacements for each layer $\{Y\}$ are

calculated using Equation (2) by the stiffness matrix $[K_a]$ and force vectors $\{F\}$, defined respectively in Equation (3) and (4). The vectors in Equations (3) and (4) are multiplied by 5 due to the 5 unit cells assembled in parallel for each layer. Here, f_i is the critical force for the respective unit cell. This is the force at the critical point corresponding to the largest slope change in the mechanical properties, such as in Figure 2(b). Similar to the unit cell uniaxial stiffness k_i^*, the critical force f_i is also extracted from unit cell FE simulation results.

$$\{Y\} = [K_a]^{-1}\{F\} \tag{2}$$

$$[K_a] = 5\begin{pmatrix} -k_1^* & k_1^* & 0 \\ k_1^* & -k_1^* - k_2^* & k_2^* \\ 0 & k_2^* & -k_2^* - k_3^* \end{pmatrix} \tag{3}$$

$$\{F\} = 5\begin{pmatrix} f_i \\ 0 \\ 0 \end{pmatrix} \tag{4}$$

Equation (2) is solved to determine the critical conditions of collapse for the 3 layer material. For multilayer materials with any number of periodic layers, only one critical point of the whole material occurs.

1.2 Functionally Graded Multilayer Material

For multilayer materials with functional gradients characterized by different unit cell designs within each layer, multiple collapse events occur, like that shown in Figure 1(c) in the main text.

The modeling approach described here simplifies the full material behavior to an equivalent piecewise linear representation, including linear elastic responses and perfect plateaus of force while the layers transition from initially collapsed to fully collapsed and thus self-contacting.

Although this modeling approach cannot precisely identify the exact critical points of collapse for each layer, the fidelity is good in comparison to the simulation as seen by comparisons presented in the main text. Given that this linear elastic network modeling requires minimal effort to compute compared to the full field FE simulation, the benefit of this first approximation can be practically significant for continued study of functionally graded elastomeric materials exhibiting collapse.

Here, the functionally graded multilayer material from the main text Figure 5(a) is used as an example. The unit cells within each layer are not identical so that $k_1^* \neq k_2^* \neq k_3^*$. A sequential modeling approach is employed on the basis of several assumptions to be defined here.

For the first critical point that occurs in this functionally graded material, Equations (1) to (4) are used, including all of the appropriate unit cell stiffnesses determined from respective FE simulations. To determine the second and third critical points, the force plateau, where displacement increases without significant change in force, must be approximated. To determine this displacement span, a simplified geometric method is used as illustrated in **Figure** S1. It is assumed that the span of force plateau displacement d_i is equal to the difference of height of the crossed beams and the height of the compacted cross beam mass. The height of the compacted cross beam mass is shown in Figure S1. This height is determined by assuming the cross beam mass is fully compressed into a rectangular shape identified by the red dashed box in Figure S1 at the fully compacted state. By geometric equality of the uncompressed and fully compressed areas, these assumptions lead to the area of the crossed beams A_i, calculated in Equation (5), and subsequently to the force plateau displacement d_i in Equation (6),

$$A_i = (2h\frac{a_i}{\cos(45)}) - a_i^2 \tag{5}$$

$$d_i = (h - Y_{i1}) - (A / w) \tag{6}$$

Here a_i is the crossed beam thickness and Y_{i1} is the critical displacement of the respective layer. This approximation for d_i assumes that once the critical force of a given layer is reached, the layer of the collapsing unit cells is the only layer that exhibits deformation within the whole functionally graded material. This assumption is warranted on the basis of the simulation and experimental results, such as in Figure 1(c,e), that demonstrate the collapse of a layer results in near total compaction of that respective layer. We also identify c_1^* as the uniaxial stiffness of the unit cell after being fully compacted. This stiffness is determined by the post-collapsed slope of the corresponding unit cell FE simulation.

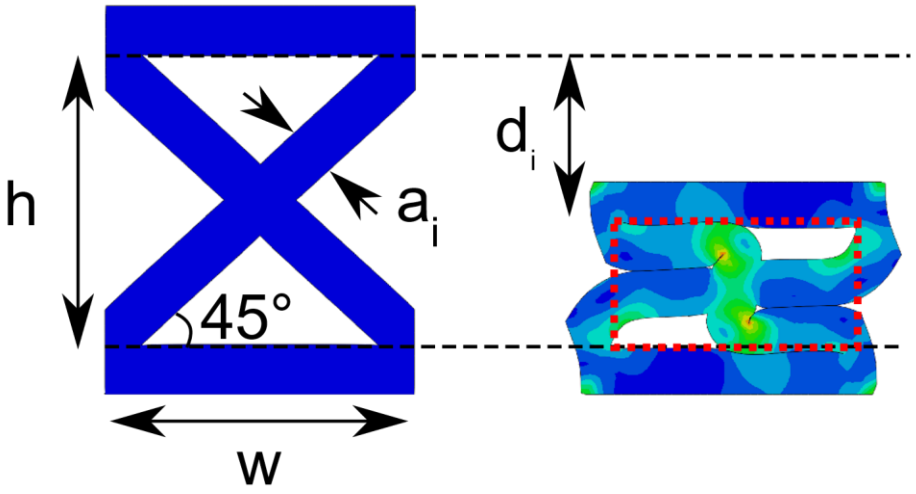

Figure S1. Schematic of the geometric method used to approximate the force plateau displacement.

The deformations in the subsequent linear elastic deformation regime of the graded material are determined through Equations (7) to (9). In Equation (9), f_2 is the critical force of the unit cell in the second layer. The force $k_2(Y_{12} - Y_{13})$ is subtracted from f_2 to account for the force exerted on

the system from the first linear regime, yielding the force f_2^*. The next critical force of collapse that occurs in the mechanical properties for uniaxial compression is therefore $f_1 + f_2^*$, **Figure** S2.

$$[K_a] = 5\begin{pmatrix} -c_1^* & c_1^* & 0 \\ c_1^* & -c_1^* - k_2^* & k_2^* \\ 0 & k_2^* & -k_2^* - k_3^* \end{pmatrix} \tag{7}$$

$$\{F\} = 5\begin{pmatrix} f_2^* \\ 0 \\ 0 \end{pmatrix} \tag{8}$$

$$f_2^* = f_2 - k_2(Y_{12} - Y_{13}) \tag{9}$$

The process repeats for subsequent layers. For the functionally graded material example with 3 layers, the final collapse behaviors are characterized by Equations (10) to (12).

$$[K_a] = 5\begin{pmatrix} -c_1^* & c_1^* & 0 \\ c_1^* & -c_1^* - c_2^* & c_2^* \\ 0 & c_2^* & -c_2^* - k_3^* \end{pmatrix} \tag{10}$$

$$\{F\} = 5\begin{pmatrix} f_3^* \\ 0 \\ 0 \end{pmatrix} \tag{11}$$

$$f_3^* = f_3 - k_3(Y_{13} + Y_{23}) \tag{12}$$

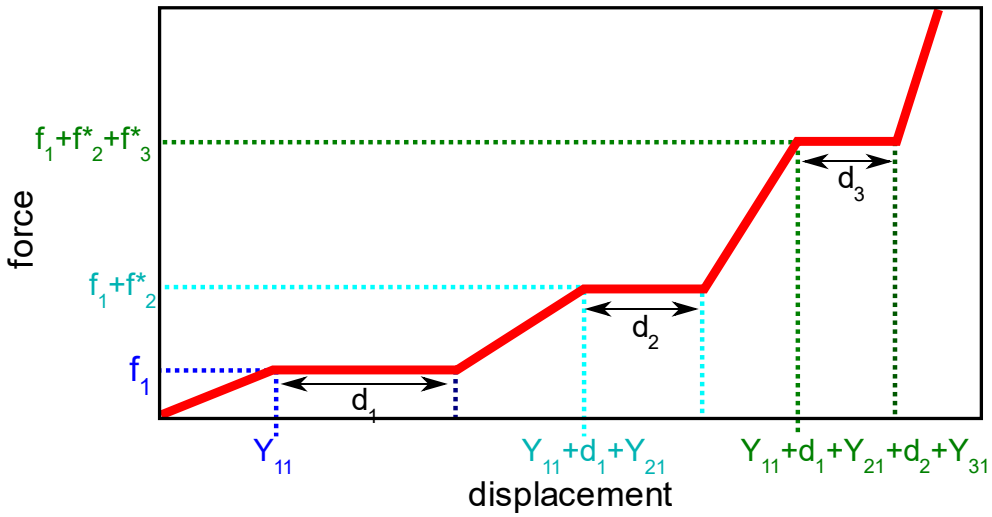

Figure S2. Illustration of the resulting critical displacement and force using the piecewise defined model.